Active Site Mutations in CheA, the Signal-Transducing Protein Kinase of the Chemotaxis System in *Escherichia coli*†

Ann Hirschman,‡ Marina Boukhvalova,‡ Ricaele VanBruggen,‡ Alan J. Wolfe,§ and Richard C. Stewart*,‡

Department of Cell Biology and Molecular Genetics, University of Maryland, College Park, Maryland 20742, and Department of Microbiology and Immunology, Stritch School of Medicine, Loyola University Chicago, 2160 South First Avenue, Maywood, Illinois 60153

Received June 28, 2001; Revised Manuscript Received September 28, 2001

ABSTRACT: We investigated the functional roles of putative active site residues in *Escherichia coli* CheA by generating nine site-directed mutants, purifying the mutant proteins, and quantifying the effects of those mutations on autokinase activity and binding affinity for ATP. We designed these mutations to alter key positions in sequence motifs conserved in the protein histidine kinase family, including the N box (H376 and N380), the G1 box (D420 and G422), the F box (F455 and F459), the G2 box (G470, G472, and G474), and the "GT block" (T499), a motif identified by comparison of CheA to members of the GHL family of ATPases. Four of the mutant CheA proteins exhibited no detectable autokinase activity (Kin^-). Of these, three (N380D, D420N, and G422A) exhibited moderate decreases in their affinities for ATP in the presence or absence of Mg^{2+}. The other Kin^- mutant (G470A/G472A/G474A) exhibited wild-type affinity for ATP in the absence of Mg^{2+}, but reduced affinity (relative to that of wild-type CheA) in the presence of Mg^{2+}. The other five mutants (Kin^+) autophosphorylated at rates slower than that exhibited by wild-type CheA. Of these, three mutants (H376Q, D420E, and F455Y/F459Y) exhibited severely reduced k_{cat} values, but preserved K_M^{ATP} and K_d^{ATP} values close to those of wild-type CheA. Two mutants (T499S and T499A) exhibited only small effects on k_{cat} and K_M^{ATP}. Overall, these results suggest that conserved residues in the N box, G1 box, G2 box, and F box contribute to the ATP binding site and autokinase active site in CheA, while the GT block makes little, if any, contribution. We discuss the effects of specific mutations in relation to the three-dimensional structure of CheA and to binding interactions that contribute to the stability of the complex between CheA and Mg^{2+}-bound ATP in both the ground state and the transition state for the CheA autophosphorylation reaction.

CheA, an autophosphorylating protein histidine kinase (PHK)[1] (*1*−*3*), plays a central role in the chemotaxis system of *Escherichia coli* (*4*, *5*), *Salmonella typhimurium* (*6*), and numerous other eubacteria (*7*−*10*) and archaea (*11*, *12*). These microorganisms use this system to modulate their swimming behaviors in response to gradients of beneficial and noxious chemicals encountered in their environments. By controlling their swimming patterns in this manner, these microorganisms can migrate toward the most beneficial location (*13*−*17*). CheA functions as an essential component of the signal transduction pathway that mediates these directed movements. In this pathway, CheA specifically regulates, via phosphorylation, the activity of a downstream effector protein, CheY (*2*). Phosphorylated CheY, in turn, interacts with the flagellar motor to control the direction of flagellar rotation, which determines the swimming pattern of the cell (*18*, *19*). CheA accomplishes phosphorylation of CheY in a two-step process (*2*). (i) In an autophosphorylation reaction, CheA interacts with ATP and catalyzes formation of P-CheA (eq 1), and (ii) in a phosphotransfer reaction, P-CheA passes its phosphoryl group to CheY (eq 2).

$$\text{CheA} + \text{ATP} \rightarrow \text{P-CheA} + \text{ADP} \quad (1)$$

$$\text{P-CheA} + \text{CheY} \rightarrow \text{CheA} + \text{P-CheY} \quad (2)$$

Both reactions require a divalent metal ion, with Mg^{2+} being more effective than alternatives (*20*, *21*).

The detailed biochemical mechanisms by which CheA catalyzes these reactions remain unknown. In the work described here, we investigated the mechanism of the CheA autophosphorylation reaction (eq 1) by examining the effects of site-directed mutations that alter putative elements of the active site that are responsible for CheA's autokinase activity.

The CheA → CheY signaling circuit is one of the best characterized examples of a "two-component" sensory response pathway, used extensively by numerous microorganisms and some higher plants to mediate responses to environmental signals (*22*). Although the details of the signaling circuitry can vary from one system to another, each two-component pathway utilizes two key signaling proteins: a protein histidine kinase (PHK) and a cognate phospho-accepting response regulator protein (RR). To

† This research was supported by Grants GM52583 (to R.C.S.) and GM46221 (to A.J.W.) from the National Institutes of Health.

* To whom correspondence should be addressed. Phone: (301) 405-5475. Fax: (301) 314-9489. E-mail: rs224@umail.umd.edu.

‡ University of Maryland.

§ Loyola University Chicago.

[1] Abbreviations: P-CheA, phosphorylated CheA; PHK, histidine protein kinase; TNP-ADP, 2′(3′)-*O*-(2,4,6-trinitrophenyl)adenosine 5′-diphosphate; IPTG, isopropyl β-D-thiogalactopyranoside.

10.1021/bi0113622 CCC: $20.00
Published on Web 10/26/2001

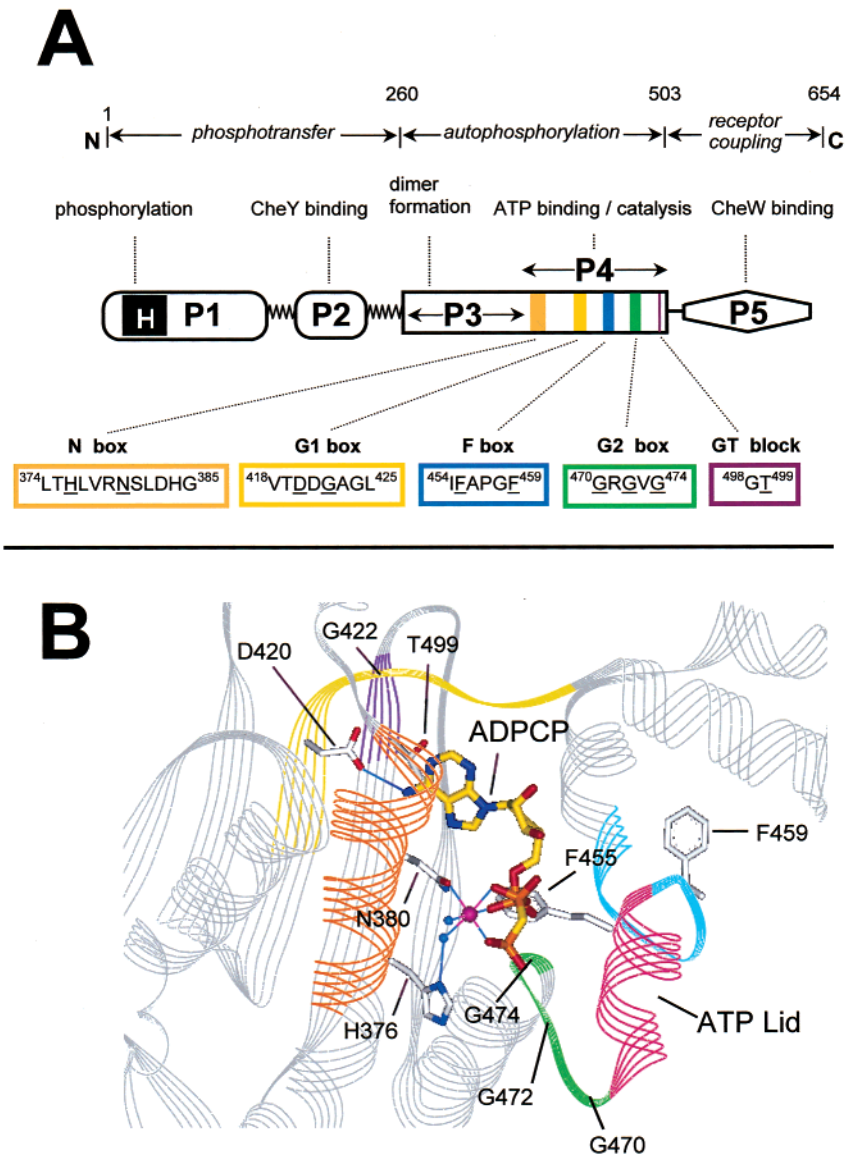

FIGURE 1: (A) Functional organization of CheA. The indicated domains (P1−P5) are those defined in structures deduced by X-ray methods (P3−P5) (*1*) and by NMR methods (P1 and P2) (*77*, *78*). The functions of these individual domains or combinations of domains have been defined by a variety of different approaches (*1*, *13*, *23*, *27*, *30*, *41*, *79*). Within P4, there are five regions containing sequences that are conserved in two-component PHKs. These regions are designated as the N box, G1 box, F box, G2 box, and GT block. The positions subjected to mutagenesis in this work are underlined. (B) Conserved residues in the ATP binding pocket of CheA and their location in relation to Mg^{2+}-bound ADPCP. The conserved boxes are labeled as follows. The G1 box is yellow with G422 and the side chain of D420 shown. The GT block is purple with the side chain of T499 shown. The N box is colored orange with the side chains of N380 and H376 depicted. The flexible "ATP lid" portion is in pink with the G2 box in green and the F box in blue flanking the region. Side chains of the two conserved phenylalanine residues in the F box are shown. ADPCP is shown bound in the active site with Mg^{2+} in magenta and two coordinated H_2O molecules depicted as small blue spheres. Hydrogen bonds are depicted as thin blue lines, from D420 to the adenine NH_2 group of ADPCP and from H376 to one of the H_2O molecules located in the Mg^{2+} coordination sphere. This drawing was created using MS Viewer Pro (Molecular Simulations, Inc.) and three-dimensional coordinates kindly provided by A. Bilwes and M. Simon (*43*).

accomplish autophosphorylation, the PHK binds Mg^{2+}-bound ATP and then catalyzes transfer of the γ-phosphoryl group from ATP to a specific histidine residue; this phosphoryl group then is transferred to the RR, eliciting a conformational change that alters the activity of the RR in a manner that generates an appropriate response. Structural information (*1*, *23*−*25*), biochemical investigations (*26*−*28*), and extensive mutagenesis studies (*29*−*32*) have made CheA one of the best characterized members of the PHK family and an excellent model for exploring the mechanism of PHK autophosphorylation and the nature of the active site that catalyzes this reaction.

CheA and other PHKs are homodimers (*33*, *34*), and the autophosphorylation reaction likely occurs via a trans mechanism in which the active site of one CheA monomer directs phosphorylation of its partner in the dimer (*35*, *36*). CheA possesses a modular architecture (depicted in Figure 1A), in which different structural elements contribute distinct functions to the overall activity and regulation (*1*, *25*, *27*). Some features of this modular organization are observed in all PHKs, while other features appear to reflect specialized elaborations on the basic PHK design to accommodate the specialized needs of the chemotaxis system (*37*). In all PHKs, the centrally located "catalytic domain" is comprised of two

structural domains, called P3 and P4 in CheA. P3 mediates dimerization of the protein, while P4 encompasses the active site that binds ATP and directs phosphorylation of a specific histidine side chain (*3*, *28*, *38*). In CheA, the phosphorylation site (His^{48}) resides in a domain (P1) distinct from the catalytic domain, while in most other PHKs, the phospho-accepting histidine is located in the dimerization domain (equivalent to P3 in CheA). CheA has a specialized domain (P2) that mediates binding to its cognate RRs (CheY and CheB) (*27*, *39*) and that facilitates rapid CheA → CheY/CheB phosphotransfer (*40*).

Several complementary approaches have helped to define the location of the autokinase active site within the P4 domain of CheA. First, sequence comparisons of CheA and many other PHKs indicate the presence of four conserved blocks termed the N box, G1 box, F box, and G2 box in P4 (*13*, *41*, *42*), as depicted in Figure 1A, and two of these blocks (G1 and G2) have characteristics similar to those of glycine-rich loops found in well-characterized kinases and nucleotide-binding proteins (*1*, *43*, *44*). Second, the three-dimensional structures of two PHKs, CheA from *Thermotoga maritima* (*1*, *43*) and EnvZ from *E. coli* (*45*), indicate that these conserved PHK "boxes" form the edges of the ATP-binding pocket, as depicted in Figure 1B. The crystal structure of the nucleotide-bound P4 domain of CheA from *T. maritima* indicates that side chains and backbone groups from specific positions within N, G1, F, and G2 are positioned appropriately for H-bonding to different moieties of the bound nucleotide (*43*). These conserved elements also mediate binding of AMP-PNP to EnvZ (*45*), but some potential differences exist in the details of specific protein−nucleotide contacts and in the conformation of the bound nucleotide compared to the CheA (P4)−nucleotide complex (*43*, *45*).

The structure of the protein fold that forms the ATP-binding site in CheA and other PHKs resembles that observed in the nucleotide-binding sites of members of the GHL family, namely, Gyrase (*46*), Hsp90 (*47*), and MutL (*48*). These proteins (*49*) function as ATPases rather than kinases, but there are some striking structural similarities between PHKs and GHL ATPases, suggesting that these protein families are related evolutionarily and may utilize similar mechanisms for binding and utilizing ATP (*1*). In addition, the GHL ATPases possess blocks of conserved amino acid sequence corresponding to the N, G1, and G2 boxes (but not the F box) of the PHKs, and specific amino acids within these boxes appear to form H-bonds with bound nucleotide in the crystal structures of the GyrB·ADPnP complex (*46*), the Hsp90·ATP complex (*47*), and the MutL·ADP complex (*48*). These sequence and structure similarities predict that conserved positions within N, G1, and G2 of CheA function in ATP binding.

Structural information about CheA, EnvZ, and the GHL ATPases has been extremely useful for identifying potential components of the CheA active site, but such assignments rest on the assumption that the location of side chain or backbone groups in the proximity of bound ATP (e.g., "within H-bonding distance") identifies these groups as functional components of the active site. Structure−function studies in other enzymes have clearly demonstrated that defining the functional roles of active site groups requires detailed biochemical characterizations of site-directed mutants to test specific predictions derived from structural analysis (*50*−*53*). We have followed such an approach to investigate the functional roles of putative active site groups in CheA. Here, we report our characterization of nine site-directed mutations that alter highly conserved positions in the well-known N, G1, F, and G2 boxes of CheA, and in a less well-known region we call the "GT block" (*48*). We investigated the effects of these mutations on the kinetic properties of CheA in autokinase assays and on the affinity of CheA for ATP in fluorescence-monitored titrations.

Previous investigations showed that mutations altering the G1, F, or G2 box of CheA and the N, G2, or F box of EnvZ eliminate or severely reduce autokinase activity (*31*). Our studies extend these previous investigations in three significant ways: (i) by examining a larger set of mutations, including some affecting the N box and GT block (previously uncharacterized in CheA); (ii) by defining the effect of each mutation not only on autokinase activity but also on ATP binding affinity and on interactions of the CheA·ATP complex with Mg^{2+}, and (iii) by relating our results to detailed structural information concerning the CheA active site available from X-ray structures (*1*, *43*).

EXPERIMENTAL PROCEDURES

Materials. 2′(3′)-*O*-(2,4,6-Trinitrophenyl)adenosine 5′-diphosphate (TNP-ADP) was purchased from Molecular Probes, Inc. (Eugene, OR), stored at −20 °C in the dark, and utilized under minimal lighting conditions. The TNP-ADP concentration was determined spectrophotometrically, based on an extinction coefficient of 26.4 mM^{-1} cm^{-1} at 408 nm (*54*). ADP and high-purity ATP were purchased from Pharmacia and Boehringer Mannheim. [γ-^{32}P]ATP was purchased from Dupont, NEN. All other chemicals were reagent grade and were purchased from standard commercial sources.

Mutant Variants of CheA. Site-directed mutations were generated by PCR megaprimer mutagenesis utilizing *Taq* DNA polymerase or *Pfu* DNA polymerase (*55*, *56*). Mutations were confirmed by DNA sequencing (performed at the University of Maryland Center for Agricultural Biotechnology).

Bacterial Strains and Plasmids. Strains RP3098 [Δ(*flhA-flhD*) (*5*)] and RP9535 [Δ*cheA* (*57*)] are derivitives of *E. coli* K-12 and were kindly provided by J. S. Parkinson (University of Utah, Salt Lake City, UT). The chromosome of RP3098 carries a deletion that removes all of the *che* genes. This strain was used for plasmid-directed overproduction of wild-type CheA and mutant variants of CheA. The overproducing plasmid used for protein production is a derivative of pAR1:cheA (*36*) modified to incorporate an N-terminal $(His)_6$ tag to facilitate purification of the proteins. Previous work demonstrated that the $(His)_6$ tag does not affect the autokinase activity or ATP binding affinity (*58*).

Protein Purification. Cultures (4 L) of RP3098 carrying pAR1:cheA were grown in Luria broth containing 100 μg/mL ampicillin. Overproduction of wild-type or mutant CheA proteins was induced by adding 1 mM IPTG to cultures in early exponential phase. Four to six hours after induction, cell pellets were collected by centrifugation and lysed by sonication. CheA was purified from cell lysates following previously published procedures: ammonium sulfate pre-

cipitation (*21*), anion exchange chromatography (*59*), and Ni−NTA chromatography (*60*). Affi-Gel Blue chromatography, an early step in the published purification procedure for the wild type (*21*), was omitted because many of the mutant proteins did not bind to this column, perhaps because they were defective in ATP binding affinity. Purified CheA preparations were stored in concentrated form (50−80 μM) at −80 °C in TEGDK buffer (*2*), and were dialyzed into TEDK buffer (i.e., lacking glycerol) immediately before being used. For some experiments, $MgCl_2$ was added (final concentration of 10 mM) immediately before use. Concentrations of purified proteins were determined spectrophotometrically, using extinction coefficients calculated by the method of Gill and von Hippel (*61*).

Swarm Assays. Tryptone swarm plates (*16*, *62*) contained 0.25% Difco Bacto agar in tryptone broth (1% tryptone and 0.5% NaCl), 100 μg/mL ampicillin, and 5 μM IPTG to induce CheA expression at levels corresponding to the level of CheA present in wild-type cells (*29*). Strain RP9535, lacking the chromosomal copy of *cheA*, was transformed with pAR1:cheA derivatives expressing the wild-type allele, the mutant alleles, or no *cheA*. Fresh transformants were stabbed into the center of tryptone swarm plates, which were then incubated at 30 °C in a humid environment. The diameter of the outermost ring of each swarming colony was measured after a 9 h incubation period.

Phosphorylation Time Course Assays. All reactions were performed at 25 °C in TEDKM buffer. Autophosphorylation reaction mixtures contained 16 μM CheA and were initiated by the addition of [γ-^{32}P]ATP (~2500 cpm/pmol). Aliquots were removed at the indicated time points, quenched with 2× SDS−PAGE sample buffer, and subjected to SDS−PAGE (12% polyacrylamide gels) in a Bio-Rad minigel apparatus. Following electrophoresis, gels were dried under vacuum and analyzed using a Bio-Rad phosphoimager, as described previously (*26*, *63*).

Assays of CheA Binding to TNP-ADP and ATP. Assays of nucleotide binding to the wild-type and mutant CheA protein took advantage of the increased fluorescence exhibited by TNP-ADP when it is bound in a hydrophobic environment (*58*). CheA samples (1 μM) were prepared in TEDK or TEDKM buffer in standard 1 cm × 1 cm fluorescence cuvettes maintained at 25 °C. Fluorescence emission spectra were recorded using a Jobin Yvon-Spex Fluoromax-2 spectrofluorometer with the excitation wavelength set at 410 nm and the emission wavelength set at 541 nm. Excitation and emission monochromators were set to give slit widths of 4 nm. For analysis of titration data, the observed emission intensity of each sample was corrected for the signal due to unbound TNP-ADP (also unbound ATP in competition experiments), as well as for inner filter and dilution effects, as reported previously (*58*). Therefore, the observed fluorescence signal used to calculate K_d values represents the enhancement of fluorescence emission intensity due to formation of the complex between CheA and TNP-ADP.

To determine the affinity of each CheA variant for TNP-ADP, we monitored the fluorescence intensity of a fixed amount of CheA titrated with increasing concentrations of TNP-ADP. The TNP moiety of the fluorescently labeled ADP analogue exhibits significantly enhanced fluorescence emission intensity when bound to the active site of CheA. The data generated by these titrations defined saturation curves plotted as $\Delta F_{obs}/\Delta F_{total}$ versus the total concentration of added TNP-ADP (e.g., Figure 4). ΔF_{obs} is the observed fluorescence signal following nucleotide addition (corrected as described above), and ΔF_{total} is the maximal value of ΔF_{obs} obtained at saturation. The ΔF_{total} value for each CheA variant was measured at saturating levels of TNP-ADP; these values differed from that observed with wild-type CheA. For mutants with a very weak affinity for TNP-ADP ($K_d^{TNP-ADP} > 50$ μM), ΔF_{total} could not be determined directly but was estimated by extrapolating the hyperbolic binding curves to saturation. Using the approach described previously (*58*), we related the observed $\Delta F_{obs}/\Delta F_{total}$ values to the amount of TNP-ADP bound per CheA dimer, and the amount of free (unbound) TNP-ADP at each point in the titration. In the case of titrations without $MgCl_2$, previously published plots were used (*58*), but new calibration plots were determined for titrations in the presence of $MgCl_2$ to account for any differences in the characteristics of bound TNP-ADP. Since the F455Y/F459Y mutant exhibited differences in spectral characteristics of bound TNP-ADP, including a shift of the emission peak as well as an increase in intensity, new calibration plots were determined for this mutant both with and without $MgCl_2$. Experiments to determine calibration plots were performed as described previously (*58*).

Plots of $[TNP\text{-}ADP]_{bound}/[CheA\ dimer]$ versus $[TNP\text{-}ADP]_{free}$ (Figure 4) were then fit using eq 3 to determine the best-fit value of K_{d1}:

$$[nucleotide]_{bound}/[CheA\ dimer] = 2N_f(K_{d2} + N_f)/(K_{d1}K_{d2} + 2K_{d2}N_f + N_f^2) \quad (3)$$

In this equation, N_f is the concentration of free TNP-ADP, K_{d1} represents the macroscopic (experimentally observed) dissociation constant for binding of the first nucleotide molecule to CheA, and K_{d2} represents the observed dissociation constant for binding of the second nucleotide to the CheA dimer. For wild-type CheA and many of the mutant versions of CheA, least-squares fits of eq 3 to the titration data indicated $K_{d2} \sim 4K_{d1}$, as expected for two identical, noninteracting binding sites per CheA dimer. However, for several mutants (D420N, F455Y/F459Y, and N380D), such fits indicated K_{d2} values in the range between 0.1 and 1.1 times the value of K_{d1}, perhaps indicating a modest level of cooperativity for the two binding events. To simplify comparison of K_d values among variants in our mutant set and to circumvent the discrepancies in K_{d2} values, we focused on values of $K_{d1}^{TNP-ADP}$, and utilized this value to define ATP binding affinities as discussed below.

Experiments to determine the affinity of CheA for unmodified ATP (K_d^{ATP}) involved titrating ATP into a solution containing a mixture of CheA (1 μM) and TNP-ADP. Competition between the added ATP and the TNP-ADP resulted in a decreased concentration of the CheA·TNP-ADP complex, which was monitored by following the decrease in the fluorescence signal associated with the complex. For each competition experiment, we determined $\Delta F_{initial}$ (the starting fluorescence signal due to the CheA·TNP-ADP complex) for the starting mixture of CheA and TNP-ADP. To calculate $K_d^{TNP-ADP}$ from $\Delta F_{initial}$, we used calibration plots ($\Delta F_{obs}/\Delta F_{total}$ vs $[TNP\text{-}ADP]_{free}$) from the TNP-ADP titrations to calculate $[TNP\text{-}ADP]_{bound}$ and [TNP-

$ADP]_{free}$ values, and then we inserted subsequent calculated values into eq 4:

$$K_{d,apparent} = ([TNP\text{-}ADP]_{free}[active\ sites]_{free})/[active\ sites]_{bound} \quad (4)$$

We repeated these fluorescence measurements and calculations after each of a series of ATP additions to obtain the apparent $K_d^{TNP-ADP}$ value. These values were plotted as $K_{d,apparent}$ versus [ATP] (Dixon plots in Figure 6) and fit using eq 5 to determine K_d^{ATP}:

$$K_{d,apparent} = K_{d1}^{\circ}(1 + [ATP]/K_{d,ATP}) \quad (5)$$

K_{d1}° represents the value of $K_{d1}^{TNP-ADP}$ in the absence of competing ATP (*y*-intercept of the plot). To simplify analysis of competition experiments, the concentrations of TNP-ADP used in these competition experiments were chosen to ensure subsaturating conditions (<0.5 TNP-ADP molecule bound per CheA dimer). Previous work (*58*) had demonstrated that the first and second TNP-ADP molecules bound to CheA do not contribute equally to the observed fluorescence emission signal. By establishing initial conditions in which the fluorescence signal was primarily due to a monoliganded CheA·TNP-ADP complex, we avoided complications arising from multiple equilibria, unequal spectral changes, and variation among $K_{d2}^{TNP-ADP}$ values in our mutants.

RESULTS

Selection of Mutation Sites and Choices of Amino Acid Substitutions. Our set of mutants included two basic types of substitutions. First, to investigate the role of specific side chains suspected of making binding contacts with ATP, we engineered conservative or semiconservative amino acid replacements, seeking to alter or eliminate specific protein−nucleotide contacts without perturbing the active site at positions adjacent to the substitution site. Second, to investigate the importance of the flexibility and/or structural integrity of the two glycine-rich loops (G1 and G2), we introduced Gly → Ala substitutions. G1 and G2 possess sequence and structural features that resemble those found in P-loops of many other nucleotide binding proteins and kinases. In these loops, the glycines provide space and conformational flexibility that contribute to nucleotide binding and to positioning of nucleotide and active site groups to promote catalysis (*1*, *43*, *44*). Specifically in CheA's structure, glycines in these two loops adopt ϕ and ψ angles that fall outside the "allowed" regions for other amino acids (*1*). Thus, we anticipated that these nonconservative Gly → Ala replacements would affect the size, conformation, and flexibility of the CheA active site.

Initially, we chose mutation sites by comparison of the amino acid sequence of CheA to a large number of other PHKs (*41*, *42*). We sought to define the functional roles of specific highly conserved positions located in the N box, G1 box, F box, and G2 box. While this work was in progress, the X-ray structure of CheA from *T. maritima* (*1*, *43*) and the NMR-derived structure of EnvZ from *E. coli* (*45*) became available. Examination of these structures and comparisons to the GHL family of ATPases suggested specific roles for some of the conserved positions in these boxes and an additional element called the GT block (*43*). Our set of mutants includes alterations of most of the residues proposed to play direct roles in ATP binding in PHKs (*1*, *45*). The locations of these mutation sites relative to bound ATP (based on the crystal structure of the P4·Mg^{2+}-ADPCP complex) (*43*) are depicted in Figure 1B. Here, we briefly discuss the specific positions we altered in conserved PHK motifs before we proceed to summarize the results of our characterization of the mutant proteins.

The N box resides at the end of an α-helix that forms one of the edges of the ATP-binding cavity of CheA (*1*, *43*). The analogous region in the structures of EnvZ, GyrB, Hsp90, and MutL contains amino acids whose side chains appear to make binding contacts with ATP and with Mg^{2+} coordinated to the polyphosphate of ATP (*45*−*48*), roles that have also been proposed for the side chain of N380 in the N box of CheA (*43*). We investigated the effects of mutations at two positions in the N box of CheA: N380 and H376.[2] Although H376 is not part of the accepted consensus sequence of the N box (*42*), we chose to investigate the effects of mutations at this position because in previous work (*64*) we had isolated H376 mutations in screens for loss-of-function mutants. Also, the imidazole side chain of H376 is thought to be positioned appropriately for productive interactions with the phosphate groups of ATP and/or the Mg^{2+} coordinated to these phosphates (Figure 1B) (*45*, *46*, *48*).

The G1 box includes a DXG motif conserved in the PHK and GHL ATPase superfamily (*44*, *65*). Analysis of the CheA crystal structures (*1*, *43*) suggests that the carboxylate group of D420 provides a substrate binding interaction by H-bonding with the adenine amino group of ATP (Figure 1B). We investigated the effects of mutations altering D420 (D420N and D420E) as well as the effects of altering the conserved glycine (G422A). This glycine to alanine substitution is expected to alter the protein backbone conformation in G1 because of steric clashes of the alanine side chain and because alanine cannot adopt the dihedral angles observed for G422 ($\psi = -159°$, $\phi = -69°$) (*1*).[3]

The GT block was identified as a potential element in the CheA active site as a result of comparisons between the three-dimensional structures of CheA (*1*) and several well-characterized enzymes, including gyrase (GyrB) (*46*), Hsp90 (*47*), and MutL (*48*). In the crystal structures of nucleotide-bound forms of these GHL ATPases, a threonine side chain H-bonds to the adenine amino group of the bound nucleotide. This residue is located in a two-amino acid block (GT) conserved in GHL ATPases (*48*). The corresponding position in the structures of CheA, EnvZ, and other PHKs is also a GT block, suggesting that this conserved threonine (T499 in CheA) might play an analogous role in ATP binding in CheA and other PHKs (*1*). We investigated the effects of T499S and T499A mutations.

[2] We refer to active site residues according to their position in the amino acid sequence of CheA from *E. coli*. The corresponding positions of the *T. maritima* protein mentioned in structural studies are 29 greater than the corresponding *E. coli* positions for the G1 and N boxes, and 32 greater for the F and G2 boxes and the GT block (thus, H376 in $CheA^{E.\ coli}$ is equivalent to H405 in $CheA^{T.\ maritima}$).

[3] To obtain ϕ and ψ angles for the glycine residues, we utilized the three-dimensional structure of *T. maritima* CheAΔ289 with no nucleotide present (*1*). Coordinates for this structure are listed in the Brookhaven Protein Data Bank as entry 1B3Q, and angles were analyzed using Swiss-PdbViewer, version 3.7b1.

We also investigated the effects of mutations that altered conserved positions in the G2 box and F box, regions of the CheA active site thought to contribute to the "ATP lid". This lid is a loop that folds over the active site when Mg^{2+}-bound ATP binds, as seen in the structure of the P4·ADPCP complex (*43*) (Figure 1B), and in the crystal structure of nucleotide-bound GyrB (*46*). We introduced mutations into the G2 box and F box, intending to limit the conformational flexibility of this ATP lid. Previous work indicated that point mutations altering one of the three conserved glycines (G470) in the G2 box of CheA did not affect ATP binding affinity, but completely eliminated autokinase activity (*58*). To further investigate the possible role of the G2 box in ATP binding, we examined the effects of a triple mutation (G470A/G472A/G474A), expected to alter the structure of G2 and to severely limit the conformational flexibility of the G2 loop. Each of these glycines adopts dihedral angles that are not possible for alanine [G470 ($\phi = 110°$, $\psi = -2°$), G472 ($\phi = 147°$, $\psi = 179°$), and G474 ($\phi = 97°$, $\psi = 128°$)] (*1*).[3]

Many (but not all) PHKs possess a conserved F box, a short block of six amino acids (*42*) situated at the end of an α-helix that forms one of the edges of the ATP binding pocket (*1*). Despite this location, the F box does not contribute directly to interactions between CheA and bound nucleotides in the P4·nucleotide complex (*43*). GHL ATPases have a comparable helix at the corresponding position of their ATP binding pocket, but there exists no apparent conservation of specific amino acid sequence within this helix (comparing PHKs to GHL ATPases or GHL ATPases to one another). Therefore, it is not possible to use the GHL structure and function information to predict functional roles for specific side chains with the F box. Nonetheless, the location of the F box in the lid segment of the active site made it an interesting target for our studies. The two most highly conserved features of the F box are its two phenylalanine residues separated by two or three amino acids in most PHKs (*42*). Thus, we constructed and tested an F box double mutant (F455Y/F459Y).

In Vitro Characterization of Mutant CheA Proteins. As described in Experimental Procedures, we generated each *cheA* mutation by megaprimer PCR mutagenesis, expressed the protein at high levels in an *E. coli* host strain devoid of other chemotaxis proteins, and purified, to >95% homogeneity, $(His)_6$-tagged versions of the resultant mutant CheA proteins. We subjected each purified CheA mutant protein to three different assays: (a) autokinase assays, using a range of ATP concentrations (*26*), (b) fluorescence-monitored titrations to assess the binding of TNP-ADP to CheA (*58*), and (c) competitive binding experiments, in which we titrated ATP into mixtures of CheA and TNP-ADP. We repeated experiments b and c in the presence and absence of 10 mM $MgCl_2$ (e.g., Figure 5), allowing us to assess the effect of Mg^{2+} on the nucleotide binding affinity for each CheA mutant.

(i) Effects of Mutations on CheA Autokinase Activity. For the initial characterization of each mutant CheA protein, we monitored the time course of its autophosphorylation in the presence of 1 mM ATP, a concentration that is 3−4 times the value of K_M^{ATP} for wild-type CheA (*26*). Figure 2 shows time courses for a representative set of mutants compared to that observed for wild-type CheA. The results of these assays indicated that altering conserved positions in N, G1, F, and G2 caused moderate to severe reductions in the rate of CheA autophosphorylation. The T499S and T499A mutations in the GT block resulted in only relatively small reductions in this rate. Four of the mutations (N380D, D420N, G422A, and G470A/G472A/G474A) completely eliminated CheA autokinase activity or reduced it to a level below our detection limit (estimated to be ~0.1% of wild-type activity); we refer to the proteins containing these mutations as Kin^- mutants. The other five mutants (which we call Kin^+) exhibited diminished autophosphorylation kinetics, with rates ranging from 2 to 40% of that observed with wild-type CheA. These reductions in autokinase activity, and the loss of activity observed with the Kin^- mutants, could have arisen from several different types of active site defects: diminished ability of a mutant active site to bind ATP, diminished ability to utilize bound ATP because active site groups are missing or misplaced, and/or diminished ability to interact with the phospho-accepting P1 module of the protein.

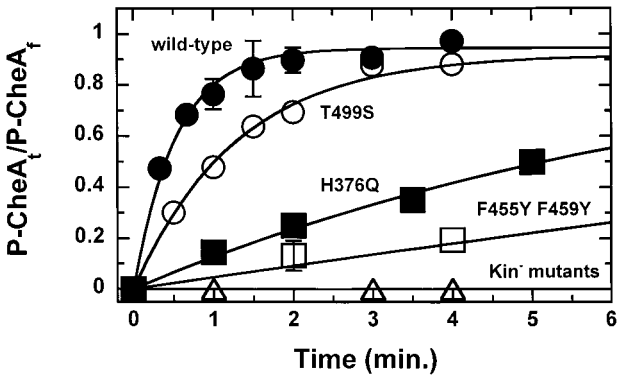

FIGURE 2: Autophosphorylation time courses for wild-type and mutant CheA variants. CheA samples (16 μM final concentration) were incubated in TEDKM buffer at room temperature with 1 mM [γ-^{32}P]ATP. Phospho-CheA levels were quantified, as described in Experimental Procedures. The fraction of final phosphorylation level plotted on the *y*-axis was defined as the ratio of [^{32}P]CheA present at the indicated time point to the final level of [^{32}P]CheA present at the reaction end point. Representative data are shown for wild-type CheA (●), T499S (○), H376Q (■), F455Y/F459Y (□), and D420N (△). Note that D420N is a mutant that exhibited no detectable autophosphorylation; an identical lack of autophosphorylation was observed for other Kin^- mutants (N380D, G422A, and G470A/G472A/G474A). For the CheA variants that did exhibit autokinase activity, the lines represent the best fits of these time courses to single exponentials and were used to determine the observed pseudo-first-order rate constants plotted in Figure 3.

To explore the specific defect(s) of each mutant protein, we examined autophosphorylation kinetics over a range of ATP concentrations (0.1−5 mM), shown in Figure 3. For the Kin^- mutants, these experiments indicated that activity could not be restored by providing ATP at much higher or lower concentrations than the 1 mM level used in the initial characterization experiments. For the Kin^+ mutants, these experiments allowed us to analyze the influence of ATP concentration on the rate of autophosphorylation, and to determine the kinetic parameters of the autophosphorylation reaction, k_{cat} and K_M^{ATP} (Table 1). Our results indicate that the severely reduced rates of autophosphorylation observed (Figure 2) for H376Q, D420E (indistinguishable from the H376Q data), and F455Y/F459Y were the result of relatively large decreases in k_{cat} (values for these mutants ranged from 0.02 to 0.1 times the k_{cat} for wild-type CheA). The com-

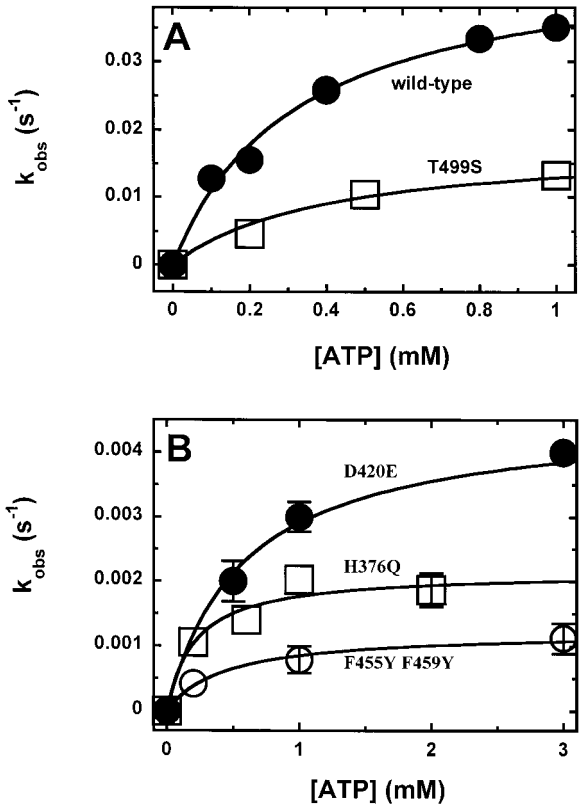

FIGURE 3: Dependence of autophosphorylation rates on ATP concentration for wild-type and mutant CheA variants. Panel A shows the relationship observed with wild-type CheA (●) and T499S (□). Panel B shows data for D420E (●), H376Q (□), and F455Y/F459Y (○). Note the different *x*- and *y*-axis scales in panels A and B. Each solid line represents the best fit of the corresponding data set to a rectangular hyperbola in defining k_{cat} and K_M^{ATP}.

Table 1: Kinetic Constants for Mutant Active Sites

	mutation location	K_M^{ATP} (mM)	k_{cat} (s^{-1})	k_{cat}/K_M^{ATP} (M^{-1} s^{-1})
wild type	NA	0.3 ± 0.1	0.050 ± 0.005	167
H376Q	N box	0.2 ± 0.1	0.0020 ± 0.0002	10
D420E	G1 box	0.6 ± 0.1	0.0050 ± 0.0002	8.3
F455Y/F459Y	F box	0.5 ± 0.1	0.0010 ± 0.0001	2
T499S	GT block	0.7 ± 0.1	0.020 ± 0.001	28.6
T499A	GT block	0.5 ± 0.1	0.023 ± 0.008	46

paratively small reduction in the autophosphorylation rate observed (Figure 2) for T499S and T499A reflected a correspondingly small reduction in k_{cat} (~40% of the wild-type value). Some of the Kin^+ mutants also exhibited small increases in K_M^{ATP} relative to that of the wild type, but these K_M effects were considerably smaller than the k_{cat} effects and did not contribute much to the time course differences observed in Figure 2.

(*ii*) *Effects of Mutations on ATP Binding Affinity.* As discussed above, we were interested in quantifying the effect of each mutation on the affinity of the CheA active site for ATP and on the ability of the active site to utilize bound ATP. With the Kin^+ mutants, analysis of autophosphorylation kinetics provided both types of information, but with the Kin^- mutants, such an approach could not be applied. Therefore, to examine ATP binding affinity with these inactive mutants, we made use of fluorescence-monitored binding titrations (*58*). We also applied this approach to the Kin^+ mutants to provide an independent measure of ATP

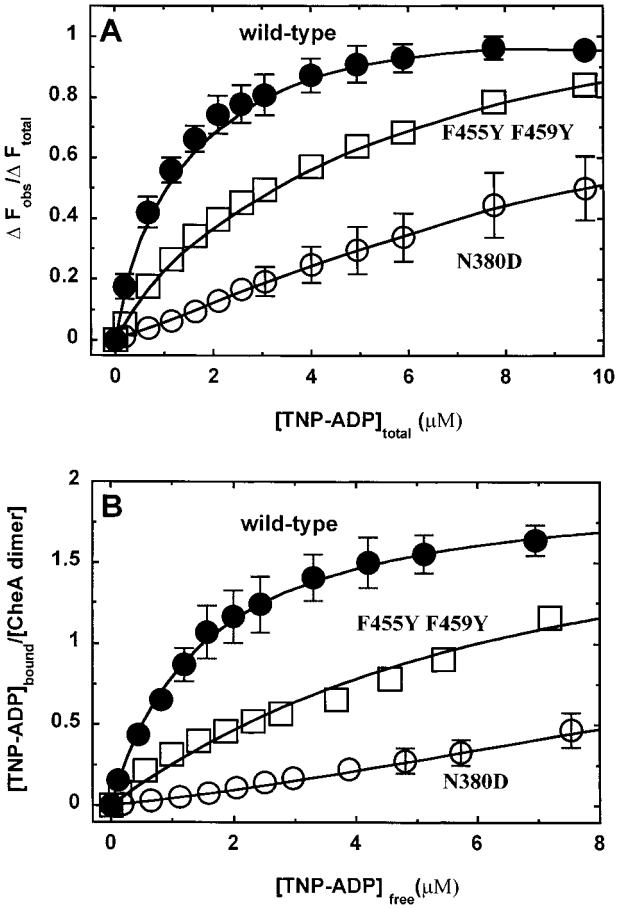

FIGURE 4: Fluorescence-monitored titration of wild-type and mutant CheA variants with TNP-ADP. Successive aliquots of TNP-ADP stock solutions were added to a 3.0 mL sample of CheA (1.0 μM) in TEDKM buffer (10 mM $MgCl_2$), and fluorescence emission intensity was recorded after each addition (λ_{ex} = 410 nm, λ_{em} = 541 nm). Plotted values were corrected as described previously (*58*). Data are shown for wild-type CheA (●), F455Y/F459Y (□), and N380D (○). Panel A displays corrected fluorescent emission intensity as a function of TNP-ADP concentration. Panel B displays the raw data converted to binding isotherms, as discussed in Experimental Procedures. Solid lines in panel A connecting data points were added to help the reader to distinguish among data sets and have no theoretical significance. The solid lines in panel B represent the curve fits according to eq 3 as discussed in Experimental Procedures.

binding affinity to compare with the K_M^{ATP} values we obtained [previous work demonstrated that $K_M^{ATP} = K_d^{ATP}$ for wild-type CheA (*26*)]. These binding experiments exploited two observations from previous work (*58*): the fluorescence emission intensity of TNP-ADP increases dramatically upon binding to CheA, and ATP competes with TNP-ADP for the CheA active site. Thus, by examining the ability of ATP to inhibit formation of the fluorescent CheA·TNP-ADP complex, we could monitor ATP binding to each of our mutant proteins.

To use this information to define K_d^{ATP} values for the mutant proteins, we first determined the value of $K_d^{TNP-ADP}$ for each mutant by analyzing the fluorescence signal observed in TNP-ADP titrations performed in the absence of competing ATP (Figure 4). The $K_d^{TNP-ADP}$ values defined by this approach (Table 2) indicated that six mutants bound TNP-ADP with diminished affinity (relative to that of wild-type CheA) and two mutants (H376Q and the G2 triple

Table 2: Effects of Active Site Mutations on the Affinity of CheA for TNP-ADP and ATP

	mutation location	$K_{d1}^{TNP-ADP}$ (μM)		K_d^{ATP} (mM)		K_d^{ATP} ratio[b]
		without Mg^{2+}	with Mg^{2+}	without Mg^{2+}	with Mg^{2+}	without Mg^{2+}/with Mg^{2+}
wild type	NA	1.2 ± 0.2	1.6 ± 0.4	1.1 ± 0.1	0.19 ± 0.01	6
H376Q	N box	0.6 ± 0.2	1.2 ± 0.2	0.9 ± 0.1	0.13 ± 0.01	7
N380D	N box	8 ± 2	50 ± 12	11 ± 3	14 ± 4	0.8
D420E	G1 box	40 ± 25	*a*	*a*	*a*	*a*
D420N	G1 box	2.3 ± 0.2	46 ± 2	4.0 ± 0.3	16 ± 5	0.3
G422A	G1 box	140 ± 80	*a*	*a*	*a*	*a*
F455Y/F459Y	F box	4.7 ± 0.3	8 ± 2	0.90 ± 0.03	0.62 ± 0.05	1.5
G470A/G472A/G474A	G2 box	0.2 ± 0.1	2.1 ± 0.04	1.4 ± 0.1	1.6 ± 0.1	0.9
T499S	GT block	3.5 ± 0.5	15 ± 2	1.5 ± 0.5	0.8 ± 0.2	1.9

[a] D420E and G422A bind TNP-ADP so poorly that we could not accurately determine K_d values via fluorescent-monitored titrations. However, for D420E, we expect that K_d^{ATP} equals K_M^{ATP}, as was seen for all other mutants. We estimate K_d^{ATP} was >100 mM for the G422A mutant, but this estimate requires several assumptions. [b] We interpreted K_d ratios (without Mg^{2+}/with Mg^{2+}) of 0.5−1.5 as indicating no effect of Mg^{2+} on CheA affinity for ATP; ratio values that were greater than this were interpreted as evidence that the mutant active site responds to Mg^{2+} in the same manner as does the wild-type active site.

mutant) exhibited binding affinities that were either indistinguishable from that of the wild type (with Mg^{2+}) or slightly stronger than that of the wild type (without Mg^{2+}). As noted in previous work, wild-type CheA binds TNP-ADP and TNP-ATP with much higher affinity than unmodified ATP (*58*). We also observed this behavior with each of our CheA mutants. One notable difference between wild-type CheA and several of the mutant proteins is that Mg^{2+} resulted in a significant *increase* (4−20-fold) in $K_d^{TNP-ADP}$ (Table 2), whereas Mg^{2+} did not affect the affinity of wild-type CheA for TNP-ADP or TNP-ATP (Table 2 and ref *58*).

To define the affinity of each mutant CheA for unmodified ATP, we performed competition experiments in which we titrated ATP into a mixture of CheA and TNP-ADP (Figure 5), and then used the resulting decreases in TNP fluorescence (due to the decreased concentration of the CheA·TNP-ADP complex) to determine K_d^{ATP}, the dissociation constant of the CheA·ATP complex, utilizing Dixon plots (Figure 6 and Table 2). For the Kin^+ mutants, the K_d^{ATP} values determined by this method match (within experimental error) the K_M^{ATP} values reported in Table 1.[4] This agreement indicates that the competition titrations provided accurate estimates of the K_d^{ATP} values. One of the four Kin^- mutants (G422A) exhibited barely detectable binding (K_d^{ATP} > 100 mM), while two of the Kin^- mutants (N380D and D420N) exhibited moderate defects in ATP binding (4−80-fold increases in K_d). Interestingly, the fourth Kin^- mutant (the G470A/G472A/G474A mutant) bound ATP with an affinity identical to that exhibited by wild-type CheA (in the absence of $MgCl_2$), suggesting that the affected region of the active site (G2) is not important for ATP binding, although the Kin^- phenotype of this mutant clearly indicates that G2 plays a crucial role in the utilization of bound ATP. A similar conclusion was reached in previous work that examined a G470K mutant (*58*).

Effects of Mutations on CheA Interactions with Mg^{2+}. In previous work, we demonstrated that Mg^{2+} enhances the affinity of CheA for ATP (*58*). We used fluorescence-monitored competition titrations (as described above) to determine whether this Mg^{2+} effect was maintained in our set of mutant proteins. As summarized in Table 2, several

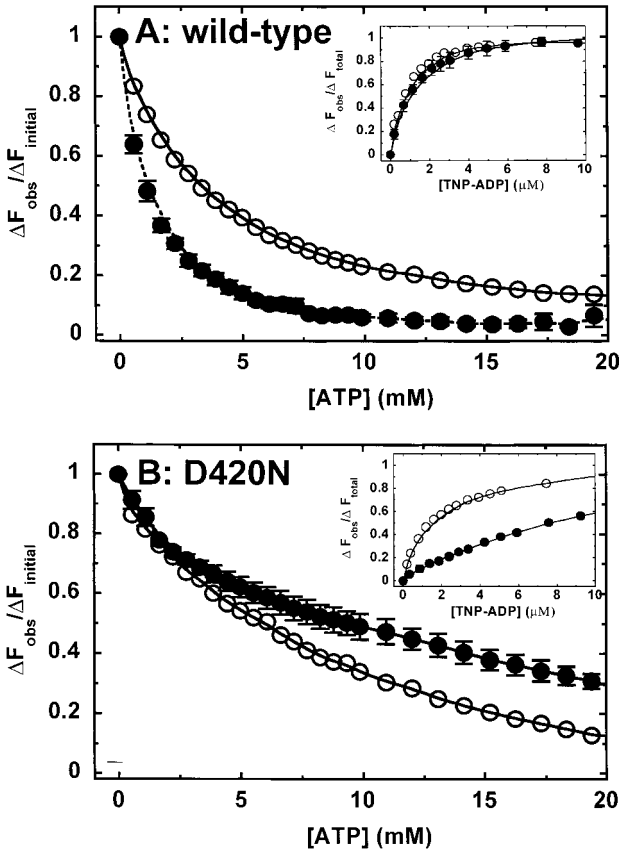

FIGURE 5: Effect of Mg^{2+} on nucleotide binding to CheA. For these ATP competition experiments (shown in the main panels), aliquots of ATP were added to a 3.0 mL sample containing 1 μM CheA and 1 μM TNP-ADP (wild type, panel A) or 2 μM TNP-ADP (D420N, panel B). Black symbols represent data from experiments in the presence of 10 mM $MgCl_2$, and white symbols represent the absence of 10 mM $MgCl_2$. Results in the main panels demonstrate that $MgCl_2$ enhances the affinity of wild-type CheA (A) for ATP and causes a small decrease in the affinity of D420N (B) for ATP. Fluorescence-monitored TNP-ADP titrations shown in the insets were performed as described in the legend of Figure 4, and demonstrate that $MgCl_2$ causes a marked decrease in the affinity of D420N (B) for TNP-ADP while $MgCl_2$ does not affect the affinity of wild-type CheA (A) for TNP-ADP. Solid lines connecting data points were added to help the reader to distinguish among data sets and have no theoretical significance.

[4] The only exception to this agreement was D420E. This mutant exhibited a K_M^{ATP} value that was twice the K_M value observed with wild-type CheA, but this mutation affected binding affinity for TNP-ADP considerably more than 2-fold ($K_d^{TNP-ADP}$ is ~40 times greater than the wild-type K_d). The affinity of D420E for TNP-ADP was even worse in the presence of $MgCl_2$, and this precluded accurate determination of K_d^{ATP} by competition methods.

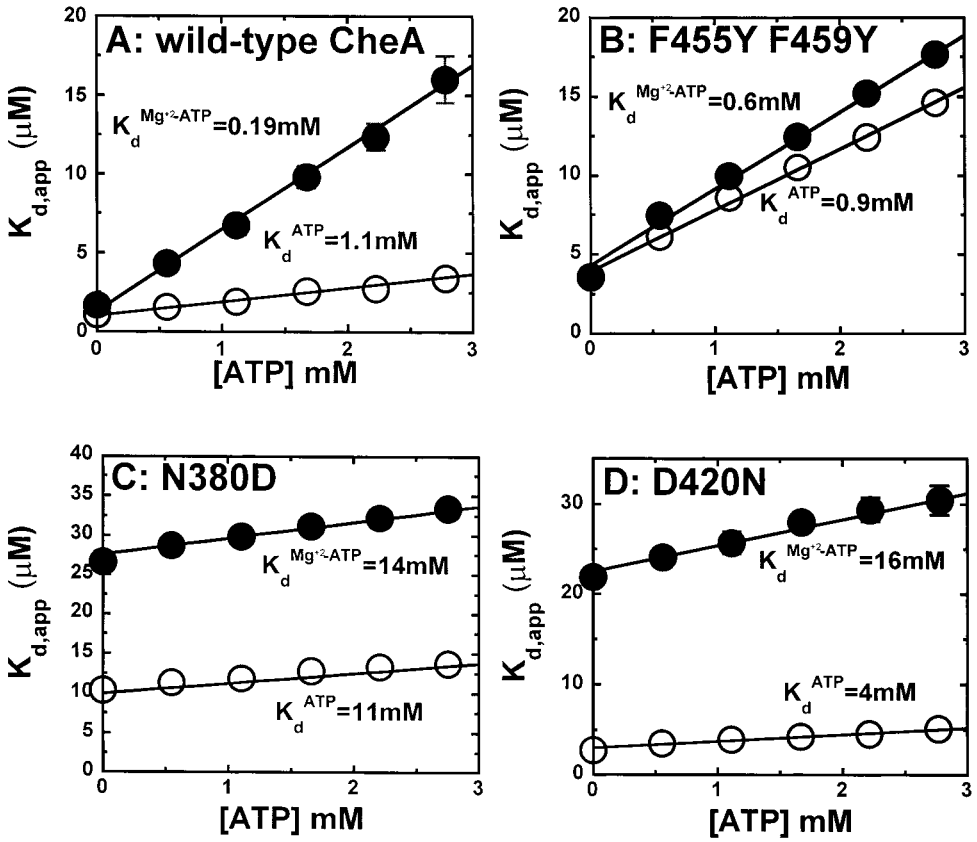

FIGURE 6: Effect of mutations on K_d^{ATP}. Dixon plots of the apparent $K_d^{TNP-ADP}$ value vs ATP concentration are shown for wild-type CheA and three mutants in the presence (black symbols) or absence (white symbols) of $MgCl_2$. The four panels are representative of four different classes of Mg^{2+} responsiveness. Panel A demonstrates the significant increase in ATP binding affinity in the presence of $MgCl_2$ for wild-type CheA. Panel B shows an example of a mutation (F455Y/F459Y) that affects ATP binding only in the presence of Mg^{2+}. Panel C shows an example of a mutation (N380D) that affects ATP binding in both the presence and absence of Mg^{2+}. Panel D shows an example of a mutation (D420N) that exhibits an inverted Mg^{2+} sensitivity.

of our mutations reduced (T499S), eliminated (N380D, F455Y/F459Y, and G470A/G472A/G474A), or even inverted (D420N) the effect of Mg^{2+} on K_d^{ATP}. As discussed in greater detail below, the loss of the Mg^{2+} effect in the G2 box mutant and the F box mutant is consistent with the suggestion (*43*) that the lid region of the CheA active site is directly involved in interactions with the polyphosphate of bound ATP and/or with the divalent metal coordinated to it. The inverted Mg^{2+} effect of the D420N mutant (Figure 5) was surprising because the side chain of D420 appears to interact with the adenine amino group of bound ATP and is not likely to interact directly with the polyphosphate−Mg^{2+} moieties of the ATP (*43*).

In the competition binding experiments performed in the presence of $MgCl_2$, we expected that wild-type CheA and the Kin^+ mutants would become phosphorylated. However, we do not anticipate that this phosphorylation had any effect on the binding results because in previous work (*58*; R. Stewart, unpublished results), we had demonstrated that K_d^{ATP} and $K_d^{TNP-ADP}$ were not affected by phosphorylation of CheA, or by a mutation (H48Q) that eliminated the autophosphorylation site.

In Vivo Complementation by CheA Proteins with Altered Active Sites. In view of the effects of some of our mutations on the in vitro autokinase activity of CheA, we deemed it of interest to determine how well the mutant CheA proteins functioned within the context of the chemotaxis signaling pathway in intact cells. We transformed plasmids expressing each *cheA* allele into a Δ*cheA* host strain and assessed the chemotactic abilities of the resulting transformants by examining their abilities to migrate in semisolid agar medium (Figure 7). Western blots confirmed that each plasmid (encoding wild-type or mutant CheA) directed expression of equal amounts of the respective CheA variants (data not shown). Not surprisingly, none of the Kin^- CheA variants (N380D, G422A, G470A/G472A/G474A, and D420N) could restore chemotactic swarming ability to the Δ*cheA* host strain. However, the active site mutants that retained partial autokinase activity (D420E, H376Q, T499S, T499A, and, to a small extent, F455Y/F459Y) partially restored chemotaxis ability. The mutant T499S exhibited no significant defect in chemotactic swarming ability, presumably because its k_{cat} value does not differ drastically from that of wild-type CheA, and because the high in vivo concentration of ATP (*66*) likely compensates for the slight K_m^{ATP} defect. Similar results were observed with T499A (data not shown). The swarming abilities of D420E (~80% of that of the wild type) and H376Q (~40% of that of the wild type) were somewhat surprising given the low k_{cat} values of these mutants.

On the basis of these observations, the chemotaxis machinery can effect signal transduction efficiently when CheA exhibits a catalytic efficiency (k_{cat}/K_M^{ATP}) that is only 5−6% of the wild-type value, but a further decrease to ~1% has severe consequences on in vivo efficacy. Several recent publications have emphasized the "robust" nature of the

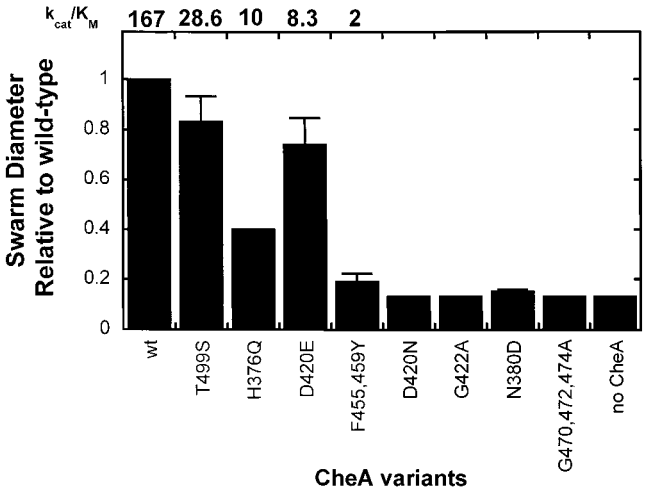

FIGURE 7: Abilities of mutant CheA variants to support chemotaxis ability. CheA proteins were expressed from an IPTG-inducible plasmid (at 5 μM IPTG) in host strain RP9535 (Δ*cheA*) (*57*). Chemotaxis ability was determined by tryptone swarm plates assays as described in Experimental Procedures. For the mutants that exhibited detectable autokinase activity, the values of k_{cat}/K_M (from Table 1) are indicated at the top of the graph. No such values could be reported for the inactive mutants (D420N, G422A, N380D, and G470A/G472A/G474A). Western blots confirmed that each plasmid (encoding wild-type or mutant CheA) directed expression of equal amounts of the respective CheA variants (data not shown).

chemotaxis signaling network; i.e., the system can tolerate relatively large fluctuations in the concentrations or activities of the signaling components without losing many of the essential output features (*67*, *68*). Our swarm assay results provide further experimental support for the general idea that effective signaling can be maintained despite a large decrease in the activity of one of the major signaling components.

DISCUSSION

Our results provide some insight into the functional roles of several specific amino acid side chains at the CheA active site and into the nature of possible contacts between some of these side chains and Mg^{2+}-bound ATP. For each such contact, there exist two potential functional roles: one role in the ground-state CheA·Mg^{2+}-ATP complex and a second potential role in the transition state for the autophosphorylation reaction. In the ground-state complex, contacts between the protein and the bound nucleotide should contribute to substrate specificity and define the value of K_d^{ATP} or K_M^{ATP} [$K_d = K_M$ for CheA (*58*)]. In the transition state, certain binding interactions between CheA side chains and Mg^{2+}-bound ATP are expected to contribute to k_{cat} by lowering the activation energy of the reaction (*69*, *70*). Although it is reasonable to expect some active site groups to contribute to both k_{cat} and K_d^{ATP}, there are numerous examples, in other enzymes, of active site groups that contribute primarily in the transition state and play relatively minor roles in ground-state binding interactions (*51*, *71*−*73*). Mutations at these sites exert large effects on k_{cat}, but not on the K_d or K_M of the enzyme−substrate complex. Conversely, some active site groups function primarily in substrate recognition and/or binding in the ground state and make little, if any, contribution to stabilization of the transition state (*51*). Mutations at these sites affect K_d (K_M) but have little influence on k_{cat}. In the following discussion, we consider the possible effects of our mutations on the ground-state CheA·ATP complex and the transition-state complex. In addition, we consider the possible impact of several mutations on interactions of CheA with Mg^{2+} and on conformational changes associated with nucleotide binding to the CheA active site. We interpret the effects of our mutations as arising from alterations of specific protein−nucleotide contacts which we judged as likely on the basis of the three-dimensional structure of the CheA·nucleotide complex (*43*). In the absence of detailed structural information for each mutant, however, we cannot rule out the possibility that nonspecific changes in active site structure or conformation contributed to the observed effects.

H376Q Is a k_{cat} Mutant. Seven of our nine mutations caused significant reductions in k_{cat}. One of these (H376Q) did so without also affecting K_d^{ATP} or K_M^{ATP} in either the presence or absence of Mg^{2+}. This finding suggests that the imidazole side chain of H376 makes a catalytically important contribution in the transition state but is not required for normal binding of ATP to the CheA active site in the ground state. Analysis of the crystal structures of P4·nucleotide complexes suggests that the side chain of H376 might play a key role in catalysis by interacting with different active site elements at distinct stages during utilization of ATP [e.g., H376 might interact with G2 in the CheA·Mg^{2+}-ATP complex, but with the β-phosphate of ADP in the CheA·ADP complex (*43*)]. These alternative interactions might play a key role in positioning G2 and other active site elements in a conformation receptive to the P1 domain of CheA (the domain that carries the phosphorylation site). Our results indicate that the contributions of H376 are important for catalysis of autophosphorylation but not for binding of Mg^{2+}-bound ATP to the CheA active site. In most PHKs, the position corresponding to H376 in CheA is occupied by glutamine or arginine. Our results indicate that it is possible for the δ-NH_2 group of Q376 in the H376Q CheA mutant to effectively substitute for the H376 imidazole group in forming a H-bond with bound ATP (*52*), thus leaving K_d^{ATP} unperturbed in the H376Q mutant, but this glutamine side chain is a poor substitute for the H376 imidazole in the interactions that promote utilization of the bound ATP.

Mutations Affecting K_d^{ATP}. Binding of ATP to the active site of CheA is expected to involve multiple H-bond contacts between the protein and the nucleotide, as depicted in Figure 1B. (Contacts with the Mg^{2+} associated with ATP are also possible, and we consider them separately below.) A mutation that disrupts one of these H-bonds (without creating an unpaired charge) is expected to increase K_d^{ATP} by 2−12.5-fold (corresponding to $\Delta\Delta G$ values of 0.5−1.5 kcal/mol) (*50*, *74*). By comparison of K_d^{ATP} values determined in the absence of Mg^{2+}, several of our mutants (N380D, D420N, and D420E) exhibited increased K_d^{ATP} values in the range expected for loss of a protein−nucleotide H-bond. Thus, the affected side chains (N380 and D420) may make stabilizing contacts with ATP in the ground-state CheA·ATP complex. These mutations also caused large decreases in k_{cat}, indicating that the affected side chains also participate in stabilization of the transition-state complex during the autophosphorylation reaction. Only one of the eight mutations (G422A) diminished the affinity of CheA for ATP by an amount that suggested disruption of numerous binding contacts; binding of TNP-ADP and unmodified ATP by the G422A mutant

was barely detectable, a result consistent with the structural analysis of Bilwes et al. (*43*), who concluded that "Gly residues in the G1 box cannot be mutated without disrupting the structure of the nucleotide binding cavity."

Effects of Mutations on Interactions with Mg^{2+}. Mg^{2+}, or some alternative divalent cation, is necessary for the autokinase activity of CheA and other PHKs (*21*). Presumably, this Mg^{2+} coordinates with the polyphosphate of the bound ATP and participates in catalysis, as in other kinases and phosphotransferases (*75*, *76*). Although CheA can bind ATP in the absence of a divalent metal, the affinity of this interaction improves approximately 5-fold in the presence of Mg^{2+} (*58*), lowering K_d^{ATP} from ~1 to ~0.2 mM. We did not observe this affinity enhancement with several of our mutants. In particular, three mutants (N380D, F455Y/F459Y, and G470A/G472A/G474A) exhibited K_d^{ATP} values that were insensitive to Mg^{2+}. In addition, one mutant (D420N) exhibited an inverted sensitivity to Mg^{2+} (K_d^{ATP} increased in response to Mg^{2+}).

How might these mutations affect CheA interactions with Mg^{2+} at a molecular level? In the crystal structure of the P4·Mg^{2+}-ADPCP complex (*43*), the six ligands occupying the octahedral coordination sphere of Mg^{2+} are (i) two water molecules that form bridges between the Mg^{2+} and the side chains of H376 and R379, (ii) three oxy ligands provided by the α-, *β*-, and *γ*-phosphates of the nucleotide, and (iii) a fourth oxygen ligand provided by the carbonyl group of the N box asparagine (N380). We anticipate that, although our N380D mutant retains a carbonyl group, the electronic and chemical properties of the carbonyl oxy group are expected to differ from those present in an asparagine carbonyl, and so it seems likely that this conservative substitution would alter, but not remove, one of the direct ligands involved in Mg^{2+} coordination to the protein−ATP complex. Our results indicate that this subtle change has consequences for both ATP binding and catalysis of CheA autophosphorylation.

We find the effects of our other mutations on CheA−Mg^{2+} interactions less easy to relate to specific structural elements of the CheA active site, because they do not directly eliminate or alter ligands in the Mg^{2+} coordination sphere. Two of our Mg^{2+}-insensitive CheA variants (the F box double mutant and the G2 triple mutant) strike us as particularly intriguing because they exerted little or no effect on K_d^{ATP} in the absence of Mg^{2+}. This finding presumably indicates that the mutant active site retains a wild-type conformation. These mutations affect a particularly interesting region of CheA, the ATP lid, a protein segment that spans F and G2 and that undergoes a dramatic conformational change upon binding of Mg^{2+}-bound ADPCP. In the absence of nucleotide, this segment acts as a relatively mobile extended loop; upon binding Mg^{2+}-bound ADPCP, this loop folds partially over the ATP-binding cavity and makes binding contacts with the polyphosphate group of the bound nucleotide (*43*). Presumably, the same events occur when CheA interacts with Mg^{2+}-bound ATP. Mutations in F or G2 might hinder the ability of the ATP lid to participate in this conformational change. Under such circumstances, the CheA active site would still interact normally with ATP in the absence of Mg^{2+}, but it would be incapable of generating the "extra binding energy" associated with closure of the lid that facilitates binding interactions to the wild-type active site in the presence of Mg^{2+}. Conformational flexibility of the ATP lid might play an important role in enabling interdomain movements that are necessary for phosphorylation of the P1 domain by the CheA active site (*43*). Our observations of a decreased k_{cat} value for an F box mutant and the loss of autokinase activity in a G2 mutant are consistent with this idea.

Summary. These studies result from limited, conservative mutagenesis of active site positions in CheA. Our results provide biochemical support for some of the functions predicted for specific amino acid side chains located in the four conserved PHK motifs of CheA. Moreover, these studies set the stage for future investigations to explore further the contributions of these active site components to catalysis of CheA autophosphorylation. For example, by generation of a larger range of substitutions at key positions and by examination of the effects of these mutations on CheA phosphorylation and dephosphorylation kinetics and nucleotide binding, it will be possible to define linear free energy profiles (*71*) for the mutant proteins and compare these to the profile for wild-type CheA. This will allow us to quantify the contributions made by various active site groups to catalysis. Relating such information to the structure of the CheA active site will eventually lead to a detailed understanding of the catalytic mechanism utilized by CheA and related PHKs and may provide important information for understanding how the activities of these enzymes are regulated to accomplish signal transduction. Moreover, detailed information about the PHK catalytic mechanism may prove to be useful for structure-based design of inhibitors that could be used as antimicrobial drugs (*43*).

ACKNOWLEDGMENT

We thank Alex Bilwes-Crane and Brian Crane (Cornell University, Ithaca, NY) as well as Mel Simon (California Institute of Technology, Pasadena, CA) for providing the coordinates of P4 complexed with ADPCP. We also acknowledge the contributions of Naureen Ali, who first identified and characterized mutations affecting H376, and Dolph Ellefson, who contributed several CheA mutants during the early stages of our work.

REFERENCES

1. Bilwes, A. M., Alex, G. A., Crane, B. R., and Simon, M. I. (1999) *Cell 96*, 131−141.
2. Hess, J. F., Oosawa, K., Kaplan, N., and Simon, M. I. (1988) *Cell 53*, 79−87.
3. Hess, J. F., Bourret, R. B., and Simon, M. I. (1988) *Nature 336*, 139−143.
4. Parkinson, J. S. (1976) *J. Bacteriol. 126*, 758−770.
5. Smith, R. A., and Parkinson, J. S. (1980) *Proc. Natl. Acad. Sci. U.S.A. 77*, 5370−5374.
6. Warrick, H. M., Taylor, B. L., and Koshland, D. E. (1977) *J. Bacteriol. 130*, 223−231.
7. Greene, S. R., and Stamm, L. V. (1999) *Gene 232*, 59−68.
8. Hamblin, P. A., Maguire, B. A., Grishanin, R. N., and Armitage, J. P. (1997) *Mol. Microbiol. 26*, 1083−1096.
9. Swanson, R. V., Sanna, M. G., and Simon, M. I. (1996) *J. Bacteriol. 178*, 484−489.
10. Ward, M. F., and Zusman, D. E. (1997) *Mol. Microbiol. 24*, 885−893.
11. Hazelbauer, G. L., Berg, H. C., and Matsumura, P. (1993) *Cell 73*, 15−22.
12. Rudolph, J., and Oesterhelt, D. (1996) *J. Mol. Biol. 258*, 548−554.

13. Stock, J. B., and Surette, M. G. (1996) in *Escherichia coli and Salmonella typhimurium* (Neidhardt, F. C., Ed.) pp 1103−1129, American Society for Microbiology, Washington, DC.
14. Berg, H. C., and Brown, D. A. (1972) *Nature 239*, 500−504.
15. Armitage, J. P. (1999) *Adv. Microb. Physiol. 41*, 229−289.
16. Adler, J. (1966) *Science 153*, 708−716.
17. Adler, J., and Templeton, B. (1967) *J. Gen. Microbiol. 46*, 175−184.
18. Welch, M., Oosawa, K., Aizawa, L.-I., and Eisenbach, M. (1994) *Biochemistry 33*, 10470−10476.
19. Welch, M., Oosawa, K., Aizawa, L.-I., and Eisenbach, M. (1993) *Proc. Natl. Acad. Sci. U.S.A. 90*, 8787−8791.
20. Lukat, G. S., Stock, A. M., and Stock, J. B. (1990) *Biochemistry 29*, 5436−5442.
21. Hess, J. F., Bourret, R. B., and Simon, M. I. (1991) *Methods Enzymol. 200*, 188−228.
22. Stock, A. M., Robinson, V. L., and Goudreau, P. N. (2000) *Annu. Rev. Biochem. 69*, 183−215.
23. McEvoy, M. M., Zhou, H., Roth, A. F., Lowry, D. R., Morrison, T. B., Kay, L. E., and Dahlquist, F. W. (1995) *Biochemistry 34*, 13871−13880.
24. Zhou, H., and Dahlquist, F. W. (1997) *Biochemistry 36*, 699−710.
25. Zhou, H., McEvoy, M. M., Lowry, D. F., Swanson, R. V., Simon, M. I., and Dahlquist, F. W. (1996) *Biochemistry 35*, 433−443.
26. Tawa, P., and Stewart, R. C. (1994) *Biochemistry 33*, 7917−7924.
27. Swanson, R. V., Schuster, S. C., and Simon, M. I. (1993) *Biochemistry 32*, 7623−7629.
28. Levit, M., Liu, Y., Surette, M., and Stock, J. (1996) *J. Biol. Chem. 271*, 32057−32063.
29. Tawa, P., and Stewart, R. C. (1994) *J. Bacteriol. 176*, 4210−4218.
30. Morrison, T. B., and Parkinson, J. S. (1997) *J. Bacteriol. 179*, 5543−5550.
31. Ellefson, D. D., Weber, U., and Wolfe, A. J. (1997) *J. Bacteriol. 179*, 825−830.
32. Bourret, R. B., Davagnino, J., and Simon, M. I. (1993) *J. Bacteriol. 175*, 2097−2101.
33. Surette, M. G., Levit, M., Liu, Y., Ninfa, E. G., and Stock, J. B. (1996) *J. Biol. Chem. 271*, 939−945.
34. Gegner, J. A., and Dahlquist, F. W. (1991) *Proc. Natl. Acad. Sci. U.S.A. 88*, 750−754.
35. Swanson, R. V., Schyster, S. C., and Simon, M. I. (1993) *Mol. Microbiol. 8*, 435−441.
36. Wolfe, A. J., and Stewart, R. C. (1993) *Proc. Natl. Acad. Sci. U.S.A. 90*, 1518−1522.
37. Dutta, R., Qin, L., and Inouye, M. (1999) *Mol. Microbiol. 34*, 633−640.
38. Garzon, A., and Parkinson, J. S. (1996) *J. Bacteriol. 178*, 6752−6758.
39. Li, J., Swanson, R. V., Simon, M. I., and Weis, R. M. (1995) *Biochemistry 34*, 14626−14636.
40. Stewart, R. C., Jahreis, K., and Parkinson, J. S. (2000) *Biochemistry 39*, 13157−13165.
41. Stock, J. B., Surette, M. G., Levit, M., and Park, P. (1995) in *Two-Component Systems* (Hoch, J., and Silhavy, T., Eds.) pp 25−52, American Society for Microbiology, Washington, DC.
42. Parkinson, J. S., and Kofoid, E. C. (1992) *Annu. Rev. Genet. 26*, 71−112.
43. Bilwes, A. M., Quezada, C. M., Croal, L. R., Crane, B. R., and Simon, M. I. (2001) *Nat. Struct. Biol. 8*, 353−360.
44. Saraste, M., Sibbald, P. R., and Wittinghofer, A. (1990) *Trends Biochem. Sci. 15*, 430−434.
45. Tanaka, T., Saha, S. K., Tomomori, C., Ishima, R., Liu, D., Tong, K. I., Park, H., Dutta, R., Qin, L., Swindells, M. B., Yamazaki, T., Ono, A. M., Kainosho, M., Inouye, M., and Ikura, M. (1998) *Nature 396*, 88−92.
46. Wigley, D. B., Davis, D. J., Dodson, E. J., Maxwell, A., and Dodson, G. (1991) *Nature 351*, 624−629.
47. Prodromou, C., Roe, S. M., O'Brien, R., Ladbury, J. E., Piper, P. W., and Pearl, L. H. (1997) *Cell 90*, 65−75.
48. Ban, C., and Yang, W. (1998) *Cell 95*, 541−552.
49. Dutta, R., and Inouye, M. (2000) *Trends Biochem. Sci. 25*, 24−28.
50. Fersht, A., Shi, J.-P., Knill-Jones, J., Lowe, D. M., Wilkinson, A. J., Blow, D. M., Brick, P., Carter, P., Waye, M. M. Y., and Winter, G. (1985) *Nature 314*, 235−238.
51. Fersht, A. R., Leatherbarrow, R. J., and Wells, T. N. C. (1986) *Trends Biochem. Sci. 11*, 321−325.
52. Leatherbarrow, R. J., and Fersht, A. R. (1987) *Biochemistry 26*, 8524−8528.
53. Tsai, M.-D., and Yan, H. (1991) *Biochemistry 30*, 6806−6818.
54. Hiratsuka, T., and Uchida, K. (1973) *Biochim. Biophys. Acta 320*, 635−647.
55. Picard, V., Ersdal-Badju, E., Lu, A., and Bock, S. C. (1994) *Nucleic Acids Res. 22*, 2587−2591.
56. Seraphin, B., and Kandels-Lewis, S. (1996) *Nucleic Acids Res. 24*, 3276−3277.
57. Liu, J. (1990) Ph.D. Thesis, University of Utah, Salt Lake City, UT.
58. Stewart, R. C., VanBruggen, R., Ellefson, D. D., and Wolfe, A. J. (1998) *Biochemistry 37*, 12269−12279.
59. Stock, A. M., Chen, T., Welsh, D., and Stock, J. (1988) *Proc. Natl. Acad. Sci. U.S.A. 85*, 1403−1407.
60. Hoffman, A., and Roeder, R. G. (1991) *Nucleic Acids Res. 19*, 6337−6338.
61. Gill, S., and von Hippel, P. H. (1989) *Anal. Biochem. 182*, 319−326.
62. Wolfe, A. J., and Berg, H. C. (1989) *Proc. Natl. Acad. Sci. U.S.A. 86*, 6973−6977.
63. Stewart, R. C. (1997) *Biochemistry 36*, 2030−2040.
64. Ali, N. (1999) Undergraduate Honors Thesis, University of Maryland, College Park, MD.
65. Stock, J. B., Ninfa, A. J., and Stock, A. M. (1989) *Microbiol. Rev. 53*, 450−490.
66. Bochner, B. R., and Ames, B. N. (1982) *J. Biol. Chem. 257*, 9759−9769.
67. Alon, U., Surette, M. G., Barkai, N., and Leibler, L. (1999) *Nature 397*, 168−171.
68. Barkai, N., and Leibler, S. (1997) *Nature 387*, 913−917.
69. Pauling, L. (1946) *Chem. Eng. News 24*, 1375−1377.
70. Haldane, J. B. S. (1930) in *Enzymes*, Longmans, Green, London.
71. Fersht, A. R., Leatherbarrow, R. J., and Wells, T. N. C. (1987) *Biochemistry 26*, 6030−6038.
72. Jencks, W. P. (1975) *Adv. Enzymol. 43*, 219−410.
73. Fersht, A. R., Knill-Jones, J. W., Bedouelle, H., and Winter, G. (1988) *Biochemistry 27*, 1581.
74. Creighton, T. E. (1993) in *Proteins*, Freeman, New York.
75. Price, N. C., and Stevens, L. (1999) *Fundamentals of Enzymology*, 3rd ed., Oxford University Press, New York.
76. Taylor, S. S., Knighton, D. R., Zheng, J., Eyck, L. F. T., and Sowadski, J. M. (1992) *Annu. Rev. Cell Biol. 8*, 429−462.
77. Zhou, H., Lowry, D. F., Swanson, R. V., and Simon, M. I. (1995) *Biochemistry 34*, 13858−13870.
78. Welch, M., Chinardet, N., Mourey, L., Birck, C., and Samama, J. P. (1998) *Nat. Struct. Biol. 5*, 25−29.
79. Morrison, T. B., and Parkinson, J. S. (1994) *Proc. Natl. Acad. Sci. U.S.A. 91*, 5485−5489.

BI0113622